inorganics

MDPI

Article

Zinc(II) Complexes with Dimethyl 2,2′-Bipyridine-4,5-dicarboxylate: Structure, Antimicrobial Activity and DNA/BSA Binding Study

Tina P. Andrejević [1], Ivana Aleksic [2], Jakob Kljun [3], Bojana V. Pantović [1], Dusan Milivojevic [2], Sandra Vojnovic [2], Iztok Turel [3,*], Miloš I. Djuran [4] and Biljana Đ. Glišić [1,*]

[1] Department of Chemistry, Faculty of Science, University of Kragujevac, R. Domanovića 12, 34000 Kragujevac, Serbia; tina.andrejevic@pmf.kg.ac.rs (T.P.A.); pantovic.bojana@pmf.kg.ac.rs (B.V.P.)
[2] Institute of Molecular Genetics and Genetic Engineering, University of Belgrade, Vojvode Stepe 444a, 11042 Belgrade, Serbia; ivana_aleksic@imgge.bg.ac.rs (I.A.); dusan.milivojevic@imgge.bg.ac.rs (D.M.); sandravojnovic@imgge.bg.ac.rs (S.V.)
[3] Faculty of Chemistry and Chemical Technology, University of Ljubljana, Večna Pot 113, SI-1000 Ljubljana, Slovenia; jakob.kljun@fkkt.uni-lj.si
[4] Serbian Academy of Sciences and Arts, Knez Mihailova 35, 11000 Belgrade, Serbia; milos.djuran@pmf.kg.ac.rs
* Correspondence: iztok.turel@fkkt.uni-lj.si (I.T.); biljana.glisic@pmf.kg.ac.rs (B.Đ.G.); Tel.: +386-1-47-98-525 (I.T.); +381-34-336-223 (B.Đ.G.)

Abstract: Two zinc(II) complexes with dimethyl 2,2′-bipyridine-4,5-dicarboxylate (py-2py) of the general formula [Zn(py-2py)X_2], X = Cl^- (**1**) and Br^- (**2**) were synthesized and characterized by NMR, IR and UV-Vis spectroscopy and single-crystal X-ray diffraction analysis. Complexes **1** and **2** are isostructural and adopt a slightly distorted tetrahedral geometry with values of tetrahedral indices τ_4 and τ'_4 in the range of 0.80–0.85. The complexes were evaluated for their in vitro antimicrobial activity against two bacterial (*Pseudomonas aeruginosa* and *Staphylococcus aureus*) and two fungal strains (*Candida albicans* and *Candida parapsilosis*), while their cytotoxicity was tested on the normal human lung fibroblast cell line (MRC-5) and the model organism *Caenorhabditis elegans*. Complex **1** showed moderate activity against both *Candida* strains. However, this complex was twofold more cytotoxic compared to complex **2**. The complexes tested had no effect on the survival rate of *C. elegans*. Complex **2** showed the ability to inhibit filamentation of *C. albicans*, while complex **1** was more effective than complex **2** in inhibiting biofilm formation. The interactions of complexes **1** and **2** with calf thymus DNA (ct-DNA) and bovine serum albumin (BSA) were studied to evaluate their binding affinity toward these biomolecules.

Keywords: zinc(II) complexes; pyridine-4,5-dicarboxylate esters; antimicrobial activity; cytotoxicity; anti-biofilm activity; DNA/BSA interaction

Citation: Andrejević, T.P.; Aleksic, I.; Kljun, J.; Pantović, B.V.; Milivojevic, D.; Vojnovic, S.; Turel, I.; Djuran, M.I.; Glišić, B.Đ. Zinc(II) Complexes with Dimethyl 2,2′-Bipyridine-4,5-dicarboxylate: Structure, Antimicrobial Activity and DNA/BSA Binding Study. *Inorganics* **2022**, *10*, 71. https://doi.org/10.3390/inorganics10060071

Academic Editor: Graeme Hogarth

Received: 16 April 2022
Accepted: 24 May 2022
Published: 26 May 2022

1. Introduction

Zinc is the second most abundant trace element in the human body with the highest concentrations in the prostate and parts of the eye [1]. Its presence has been estimated in different enzymes, which have a structural and a catalytic or co-catalytic role [2]. For instance, it is incorporated in the active center of superoxide dismutase (SOD), carbonic anhydrase, carboxypeptidase, and alcohol dehydrogenase [3,4]. This metal plays an essential role in the development and maintenance of the immune system, wound healing, protein syntheses, and cell division [1,5,6]. Besides that, it is essential for DNA synthesis, and repair processes have an important role in the transcription factor function and a key role in monitoring the cell's metabolism and in their protection against oxidation stress [7,8]. Zinc(II) is also required for the sense of taste and smell and for normal growth and development during pregnancy, childhood, and adolescence [1]. Due to its antioxidant properties, this metal ion protects the organism against accelerated aging and can speed up the healing after an injury [1]. Besides that, zinc(II) has a key role in synaptic plasticity and learning, as well

as in the normal functioning of the central nervous system [1]. It is important to mention the role of zinc in oncogenesis, because its levels are influenced by the cells present in the cancer microenvironment, including pro-inflammatory mast cells [9,10]. Moreover, in the mammalian pancreas, zinc(II) is required for the processing, storage, secretion, and action of insulin in β-cells [11]. Accordingly, different studies have suggested that the reduced amount of this metal ion is connected with diabetes [12,13].

Zinc is also an essential microelement for microorganisms, being a structural and catalytic cofactor in many bacterial metalloproteins, such as zinc-dependent proteinase in the cell wall of *Lactobacillus delbrueckii* subsp. *bulgaricus*, alcohol dehydrogenase isolated from *Mycobacterium bovis*, *Bacillus subtilis,* and *Helicobacter pylori,* and phospholipase C in *Bacillus cereus* [14]. At the same time, this metal inhibits the growth of different bacteria, including *Escherichia coli* and *Streptococcus faecalis* [14,15]. In this context, the concentration of zinc(II) ion is a determining factor, which has an influence on bacterial growth. Thus, at low concentrations, the promoting effect is predominant, however, at the higher concentration, this metal ion inhibits the growth of bacteria [16]. It was found that the optimal concentration of zinc(II) in microbial cells is in the range of 10^{-7} to 10^{-5} M, while the concentrations above 10^{-4} M enhance the permeability of this ion through the cell membrane, having cytotoxic effects on prokaryotes [17]. Although the concentration of zinc(II) ion has a significant influence on antimicrobial activity, the effect of the form of the zinc(II) compound itself is not negligible [18]. The exact mechanism of the antimicrobial activity of zinc(II) still remains unclear, but it is supposed to be connected with the interaction of this ion and cell membrane, leading to its destabilization and enhanced permeability, or with the interaction with the nucleic acids, which causes the dysfunctions of the respiratory enzymes [17]. Moreover, the insoluble zinc(II) compounds, such as ZnO, could induce the production of reactive oxygen species (ROS) [19].

Considering the abovementioned, zinc(II) ion is applied as a constituent of compounds which have been used as antimicrobial agents [15]. For instance, ZnO is the most widely, but not the only used zinc(II) compound in personal care formulations [17], attracting special interest in the form of nanoparticles [17,18]. Except for the oxide, different zinc(II) salts and complexes have shown remarkable antimicrobial properties [17,20], as well as lower toxic side effects compared to other metal-based drugs [8]. One of the advantages of the administration of zinc in a form of a complex instead of a simple inorganic salt is the selective delivery of zinc(II) ions to the diseased tissues, as well as the modification of pharmacokinetics and/or pharmacodynamics due to the ligands. An excellent example of an active complex is ZPT, i.e., zinc(II) complex with pyridinethione (pyrithione), which reduces the activity of pathogenic species *Pityrosporum* (*Malassezia*), being responsible for skin conditions, such as dandruff and seborrhoeic dermatitis [21]. This complex has also shown a high antibacterial activity, i.e., thermoplastic elastomers incorporated with ZPT have manifested a good inhibitory effect on *E. coli* and *Staphylococcus aureus* [22]. Furthermore, zinc(II) complexes of chlorogenic acid [23], *p*-coumaric acid, and ferulic acid [24] have demonstrated the antibacterial activity against *S. aureus*, while zinc(II) complexes with aromatic nitrogen-containing heterocycles, $[ZnCl_2(qz)_2]$, $[ZnCl_2(1,5\text{-naph})]_n$ and $[ZnCl_2(4,7\text{-phen})_2]$, (qz is quinazoline, 1,5-naph is 1,5-naphthyridine and 4,7-phen is 4,7-phenanthroline) have shown good antifungal activity against two *Candida* strains (*C. albicans* and *C. parapsilosis*), being not toxic on the normal human fibroblast cell line (MRC-5) [25]. Complex $[ZnCl_2(4,7\text{-phen})_2]$ has the ability to interfere with the yeast to hyphae transition and has shown a significant synergistic effect with the clinically used antifungal agent nystatin [25]. Moreover, it was found that zinc(II) has remarkable immunogenic properties and could help ameliorate the disease caused by COVID-19 infection [26].

In the present study, we have used dimethyl 2,2′-bipyridine-4,5-dicarboxylate (py-2py) as a ligand for the synthesis of two new zinc(II) complexes of the general formula $[Zn(py\text{-}2py)X_2]$, X = Cl^- (**1**) and Br^- (**2**). This ligand has been previously used for the synthesis of silver(I) complexes $[Ag(NO_3)(py\text{-}2py)]_n$ and $[Ag(CH_3CN)(py\text{-}2py)]BF_4$, as efficient agents for the control of cow mastitis associated pathogens [27], as well as of

copper(II) complex, $[Cu(NO_3)_2(py\text{-}2py)(H_2O)]\cdot H_2O$, which has shown the activity against the fungus *C. albicans* [28]. Furthermore, it was previously employed in the design of ruthenium complexes as potential anticancer agents [29–31]. The synthesized $[Zn(py\text{-}2py)X_2]$ complexes were characterized by spectroscopy (^{1}H NMR, IR, and UV-Vis) and single-crystal X-ray diffraction. They were assessed for in vitro antimicrobial activity against two bacterial (*Pseudomonas aeruginosa* and *S. aureus*) and two fungal (*C. albicans* and *C. parapsilosis*) strains and for cytotoxicity on MRC-5 cells, as well as for in vivo toxicity on the model organism *Caenorhabditis elegans* (*C. elegans*). The ability of the complexes to inhibit filamentation of *C. albicans* and the biofilm formation process in this fungus was also evaluated. The interactions of $[Zn(py\text{-}2py)X_2]$ complexes with calf thymus DNA (ct-DNA) and bovine serum albumin (BSA) were studied with the aim to check their binding affinity toward these potential biological targets.

2. Results and Discussion

2.1. Synthesis and Structural Characterization of the Zinc(II) Complexes **1** *and* **2**

Dimethyl 2,2′-bipyridine-4,5-dicarboxylate (py-2py) was used as a ligand for the synthesis of two new $[Zn(py\text{-}2py)X_2]$ complexes, X = Cl^- (**1**) and Br^- (**2**) (Scheme 1). Complexes **1** and **2** were characterized by elemental analysis, IR, ^{1}H NMR, and UV-Vis spectroscopy, while their crystal structures were determined by single-crystal X-ray diffraction analysis.

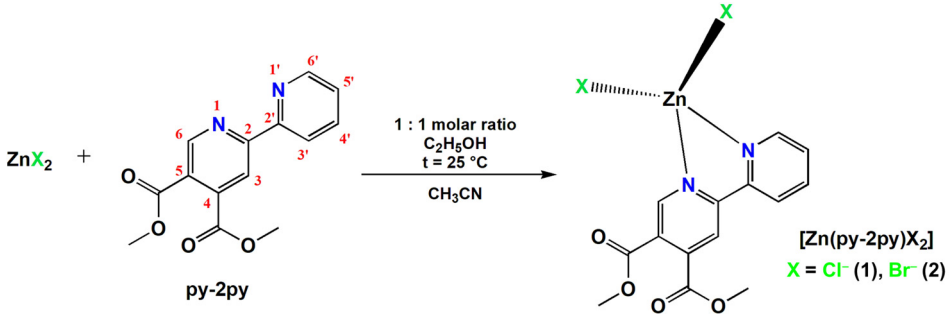

Scheme 1. Schematic presentation of the synthesis of complexes **1** and **2**. Numeration of atoms in the ligand is used for NMR characterization of the synthesized complexes.

2.1.1. Description of the Single Crystal Structures

Complexes **1** and **2** are isostructural and crystallize in the monoclinic space group *I*2/a. As expected, the inclusion of the larger halogenido ligand (bromido) leads to a slightly bigger cell volume in the case of **2**. Both complexes adopt a slightly distorted tetrahedral geometry with values of tetrahedral indices τ_4 [32] and τ'_4 [33,34] in the range of 0.80–0.85 (Figure 1 and Table 1). The distortion is attributed to the relatively low bite angle of the bipyridine ligands (approx. 80° when bound to divalent 3d metal ions). Stacking interactions (π-π and weak C–H···X; see Figure S1 in Supplementary Materials) also contribute to the distortion resulting in a slight tilt of the ZnXX (X = Cl or Br) plane from the ideal 90° angle to the ZnNN (N = N1, N7) plane. All bond lengths and angles are within the expected range of values reported in the CSD database.

2.1.2. Spectroscopic Characterization

The IR, ^{1}H NMR, and UV-Vis spectroscopic data for zinc(II) complexes **1** and **2** are listed in the Experimental section (vide infra), while the corresponding data for py-2py are given in Supplementary Materials. The IR spectra of complexes **1** and **2**, recorded in the wavenumber range of 4000–450 cm^{-1}, show the vibrations that are attributed to the coordinated py-2py ligand. Besides that, ^{1}H NMR spectra were recorded in deuterated DMSO with the aim to confirm the coordination of py-2py ligand to the Zn(II) ion in complexes **1** and **2** in solution (Figure S2 for complex **1**). For this purpose, the NMR spectra of the complexes were compared with that of the uncoordinated ligand. In both cases, the number of signals due to the py-2py in complexes was identical to that of the

uncoordinated ligand. In the aromatic region, ^{1}H NMR spectra of complexes **1** and **2** consist of six resonances corresponding to the protons H3, H6, and H3′–H6′, with chemical shifts differing from those of the free py-2py ligand (in most cases). Of particular note is the shifting of the NMR signal of the H6 proton, which is adjacent to the pyridine nitrogen binding center, as well as H5′. These protons appear at δ = 8.78 and 8.06 ppm in the spectrum of uncoordinated ligand, respectively. However, both these signals were shifted downfield at 9.05 ppm ($\Delta\delta$ = 0.27 ppm for **1**) and 9.03 ppm ($\Delta\delta$ = 0.25 ppm for **2**), and at 8.29 ppm ($\Delta\delta$ = 0.23 ppm for **1**) and 8.27 ppm ($\Delta\delta$ = 0.21 ppm for **2**), respectively, after ligand coordination to the Zn(II) ion. In the aliphatic region of the ^{1}H NMR spectra of the complexes **1** and **2**, a signal at 3.91 and 3.90 ppm, respectively, is observed, attributed to the methyl protons of the -COOCH$_3$ group [26].

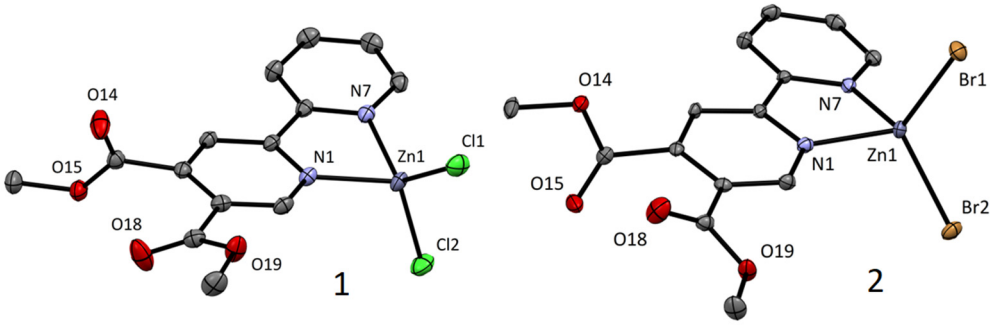

Figure 1. Crystal structures of complexes **1** and **2** with heteroatom labelling. Thermal ellipsoids are shown at 50% probability level. Hydrogen atoms are omitted. N. b. N7 notation corresponds to the N1′ notation in the IUPAC nomenclature used in NMR assignment.

Table 1. Selected bond lengths, angles and structural parameters of the crystal structures of **1** and **2**.

Compound	1	2
Zn-N1; Å	2.071(1)	2.069(3)
[a] Zn-N1′; Å	2.069(1)	2.062(3)
Zn-X; Å	2.2099(7), 2.2017(8)	2.3369(9), 2.3399(7)
X-Zn-X; °	114.58(2)	113.35(2)
[b] φ; °	81.15	80.02
[c] τ_4 [32]	0.85	0.83
[c] τ'_4 [33,34]	0.82	0.80

[a] crystallographic label of N1′ atom in the cif file is N7; [b] φ = angle between planes defined by ZnNN and ZnXX atoms; [c] $\tau_4 = [360° - (\alpha + \beta)]/(360° - 2\theta)$; $\tau'_4 = [(\beta - \alpha)/(360° - \theta)] + [(180° - \beta)/(360° - \theta)]$; α and β are the two greatest valence angles of coordination center, θ is tetrahedral angle 109.471°. For ideal square-planar geometry τ_4 and τ'_4 values are 0, for ideal tetrahedral geometry τ_4 and τ'_4 values are 1.

2.2. Solution Stability of Complexes **1** *and* **2**

The solution behavior of complexes **1** and **2** were studied by recording the UV-Vis spectra in DMSO after their dissolution, as well as after 24 and 48 h. No significant changes in the intensity and position of the absorption maxima of the investigated complexes were detected during this time, indicating the stability of the solution (Figure S3). This could be also concluded from the molar conductivity values, which are in accordance with the non-electrolytic nature of the complexes **1** and **2** in DMSO solution [35], i.e., no substitution of chloride with DMSO was observed. On the other hand, the molar conductivity measurements in DMSO/H_2O (*v*/*v* 1:9) were not conclusive, and we can only conclude that, in an aqueous environment, all complexes undergo processes of solvation, hydrolysis, and/or substitution over time.

2.3. Biological Activity Study

Zinc(II) complexes **1** and **2**, py-2py ligand, and inorganic salts used for the synthesis of both complexes were tested against two bacterial (*P. aeruginosa* and *S. aureus*) and

two fungal strains (*C. albicans* and *C. parapsilosis*). Complex **1** was the only one showing moderate antimicrobial activity with the MIC value of 62.5 μg/mL against fungal strains, while complex **2**, py-2py ligand, and inorganic salts were showing neither antibacterial nor antifungal activity at concentrations as high as 500 μg/mL (Table 2).

Table 2. Antimicrobial activity of complexes **1** and **2**, py-2py ligand and inorganic salts used for their synthesis (MIC, μg/mL), in comparison to their antiproliferative effect on the normal human fibroblast cell line MRC-5 (IC_{50}, μg/mL).

Test Organism \ Compound	**1**	**2**	**$ZnCl_2$**	**$ZnBr_2$**	**py-2py**
Pseudomonas aeruginosa NCTC 10332	>500	>500	>500	>500	>500
Staphylococcus aureus ATCC 25923	500	>500	500	500	>500
Candida albicans ATCC 10231	62.5	>500	>500	>500	>500
Candida parapsilosis ATCC 22019	62.5	>500	>500	>500	>500
MRC-5 cells	33 ± 1	75 ± 2	36 ± 1	22 ± 1	120 ± 4

Identifying potential toxicity at an early stage during drug discovery is very important because it usually saves both time and development costs. Usually, the first step in the safety assessment of a potential antimicrobial agent is a cell culture-based in vitro assay, including an MTT assay. In order to evaluate the possibility of further exploiting the antifungal effect of complex **1**, the cytotoxicity of both complexes, corresponding inorganic salts, and py-2py ligand against healthy fibroblasts was determined using MTT assay, with the IC_{50} values in the range from 22 μg/mL for $ZnBr_2$ to 120 μg/mL for py-2py. Again, more potent was complex **1** having an IC_{50} value of 33 μg/mL, compared to complex **2** with an IC_{50} value of 75 μg/mL (Table 2).

Additionally, the nematode *C. elegans* was used as in vivo model system for toxicity testing, and it was shown that both complexes and corresponding salts used for their synthesis did not have any effect on the survival rate of *C. elegans.* No death of worms has been recorded during the common incubation period of 48 h, but not even with the prolonged incubation up to 72 h (Figure S4).

Having confirmed the relative safety of tested compounds and mostly no activity against planktonic growth of selected microorganisms, complexes **1** and **2** were further tested for their ability to act as signaling molecules that could interfere with microbial processes important for pathogenesis including filamentation and biofilm formation in *C. albicans* [36,37]. It was previously shown that zinc(II) complexes with the clinically used drug fluconazole and 4,7-phenanthroline had the ability to inhibit *C. albicans* hyphae formation, the virulence factor essential for penetration of human cells during infection [25,38]. In this study, the ability of complexes **1** and **2** to inhibit filamentation of *C. albicans* was evaluated firstly on hyphae promoting Spider medium using a concentration of 50 μg/mL. At this concentration, complex **2** inhibited hyphae formation even after 72 h incubation, while none of the other tested compounds influenced hyphae formation (Figure 2). Therefore, the effects of complex **2** to influence the morphological transformation from the yeast-to-hyphae form was tested in RPMI liquid medium, as well (Figure S5). In this assay only amphotericin B, as a standard antifungal drug, completely inhibited the filamentation process, compared to the control treated with DMSO, while the inhibitory effect of complex **2** was not confirmed under these conditions.

Filamentation is an important phase during the infection process, and the early step in *C. albicans* biofilm formation [39]. Hence, complexes **1** and **2**, corresponding salts, and py-2py ligand were evaluated for the inhibition of the biofilm formation process in *C. albicans* ATCC 10231 (Figure 3). Interestingly, complex **1** showed moderate ability to inhibit biofilm formation, between 30–45% in the concentration range 7.8–31.2 μg/mL. However, complex **2** showed lower activity in comparison to complex **1** with up to 25% inhibition at 125 μg/mL. Inorganic salt $ZnBr_2$ was the most active of the tested compounds, while py-2py ligand showed no biofilm inhibition activity (Figure 3).

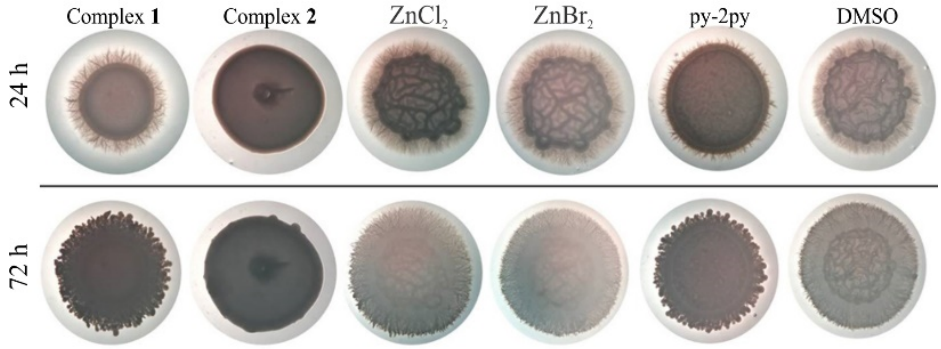

Figure 2. Colonies of *C. albicans* ATCC 10231 on Spider medium, supplemented with complexes **1** and **2**, corresponding inorganic salts and py-2py ligand (50 μg/mL) in comparison to DMSO. Colonies were photographed under a stereomicroscope (SMZ143-N2GG, Motic, Wetzlar, Germany) after 24 and 72 h of incubation.

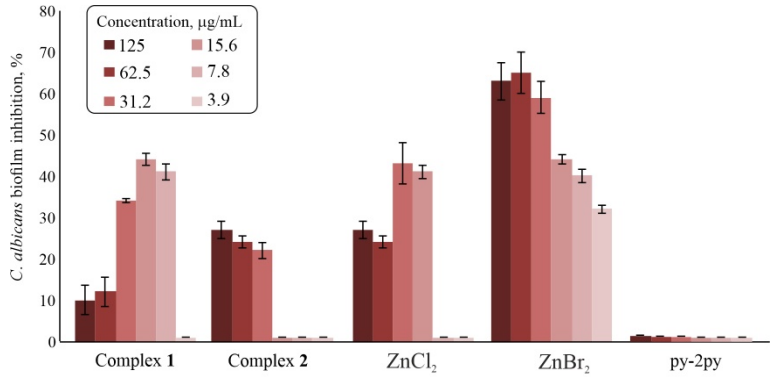

Figure 3. *C. albicans* ATCC 10231 biofilm inhibition in the presence of complexes **1** and **2**, corresponding $ZnCl_2$ and $ZnBr_2$ salts and py-2py ligand.

It has been shown that quorum sensing (QS), a bacterial cell–cell communication process, supervising the activity of processes important for microbial pathogenicity like sporulation and biofilm formation, could serve as a target for anti-virulence therapy [40]. Many QS-systems were evaluated as targets for anti-virulence therapy with different compounds [41]. The quorum sensing inhibitory potential, especially regarding bacterial pigment pyocyanin production, was demonstrated for gold(III) complexes with clinically used antifungal azoles [42]. In this study, the quorum sensing inhibitory potential of complexes **1** and **2**, corresponding inorganic salts, and py-2py ligand was tested using two biosensor strains: *Serratia marcescens* (prodigiosin producer) and *Chromobacterium violaceum* CV026 (violacein producer). Disc assays on *S. marcescens* and *C. violaceum* CV026 implicated no potency to act as quorum quenchers, apart from complex **1** which showed moderate activity on *S. marcescens* with the zone of pigment production inhibition of 8 mm (Figure S6a). Also, complex **1** and inorganic salts showed some growth inhibition towards *C. violaceum* CV026 and *S. marcescens* as well, when tested at a high concentration of 500 μg per disc (Figure S6).

2.4. DNA Interaction

As was mentioned in the Introduction, the study of the interaction of zinc(II) complexes with DNA can contribute to a better understanding of the mechanism of their antimicrobial activity. Firstly, the binding affinity of complexes **1** and **2** toward DNA was investigated by fluorescence spectroscopy by monitoring the emission intensity of ethidium bromide (EthBr) bound to ct-DNA (Figure S7). As it was known, EthBr intercalates between adjacent base pairs in the DNA double helix, resulting in the enhancement of its fluorescence [43,44]. If a tested compound intercalates into ct-DNA, a decrease in the fluorescence intensity of

the EthBr-ct-DNA system will be observed [45]. However, as can be seen from Table 3, the values of binding constants (K_A) for the complexes **1** and **2** are lower than that for EthBr ($K_A = 2 \times 10^6$ M^{-1}), suggesting that these complexes are not intercalating agents [46]. By comparison of the K_A values of the investigated complexes, it can be concluded that complex **2** has a higher binding affinity for ct-DNA than complex **1**, which can be due to the easier hydrolysis of the Zn–Br bond with respect to Zn–Cl as a consequence of the difference in the size between chloride and bromide anions and a hard character of Zn(II) ion and soft character of bromido ligand (whereas chloride is intermediate ion according to Pearson acid-base concept [47]). This is consistent with values of the number of binding sites for ct-DNA (n), which are significantly higher for complex **2** than for complex **1**. The percentage of hypochromism is very small (up to 15%), confirming the non-intercalative mode of binding. For comparison, the percentage of hypochromism of 50% was previously obtained for lucigenin, which is proven as a DNA intercalator [48]. On the other hand, the values of K_q constants indicate that the mechanism of interaction between complexes **1** and **2** and ct-DNA is a static quenching [46].

Table 3. Values of the binding constants of complexes **1** and **2** with ct-DNA.

Complex	K_{sv} (M^{-1})	Hypochromism (%)	K_q (M^{-1} s^{-1})	K_A (M^{-1})	n
1	$(9.28 \pm 0.01) \times 10^2$	14.8	9.28×10^{10}	14.2	0.49
2	$(1.73 \pm 0.01) \times 10^3$	14.4	1.73×10^{11}	7.77×10^4	1.45

The interaction of the complexes with DNA was also observed in a gel electrophoresis assay (Figure 4). The investigated compounds were added to a concentration of 500 μg/mL and incubated with the λDNA at 37 °C, and after 2, 4, and 24 h of incubation, samples were stained with EthBr, loaded into wells, and electrophoresis was conducted (Figure 4). No influence of DMSO, water, and ligand py-2py on λDNA was observed, as the bands for these samples remained highly concentrated, while for complexes **1** and **2** and ZnX_2 salts, the DNA band on gel electrophoresis was obviously thinner, suggesting that these compounds prevented EthBr intercalation. The trend of getting thinner after longer incubation time implicates the effects of complexes on DNA structure and stability. In accordance with this, the activity of the complexes was observable even after 4 h of incubation, while py-2py ligand did not have any effect on the DNA even after 24 h of incubation.

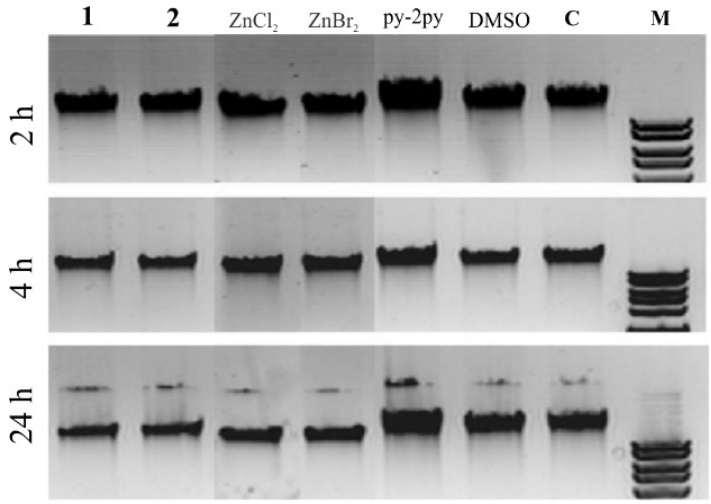

Figure 4. In vitro interaction of complexes **1** and **2**, $ZnCl_2$ and $ZnBr_2$ salts and py-2py with λDNA assessed by gel electrophoresis in comparison with DMSO and H_2O (C) treatments after 2, 4 and 24 h of incubation. M denotes standard DNA marker peqGOLD 1 kb DNA-Ladder Plus with 10 kbp largest band.

2.5. Protein Binding Study

2.5.1. Fluorescence Emission Spectroscopy

The studies of the binding interaction of metal complexes with proteins are of great importance for a better understanding of the mechanism of their uptake, transport, metabolism, and toxicity [43]. One of the most studied proteins is serum albumin (SA), which is present in the blood plasma and plays an important role in the transport and delivery of an active compound to the target cells [43]. Bovine serum albumin (BSA) is the most extensively studied serum albumin, while fluorescence spectroscopy is one of the most convenient methods for the investigation of BSA interactions with metal complexes. The fluorescence quenching of BSA after its interaction with a metal complex indicates the change in its conformation, the interaction with a studied compound, or the protein denaturation [49].

The emission spectra of BSA were recorded in the absence and presence of an increasing amount of the investigated zinc(II) complexes (Figure 5). A significant decrease of fluorescence intensity was observed upon the addition of an increasing concentration of complexes **1** and **2** to BSA solution of a constant concentration, as a consequence of their binding to BSA.

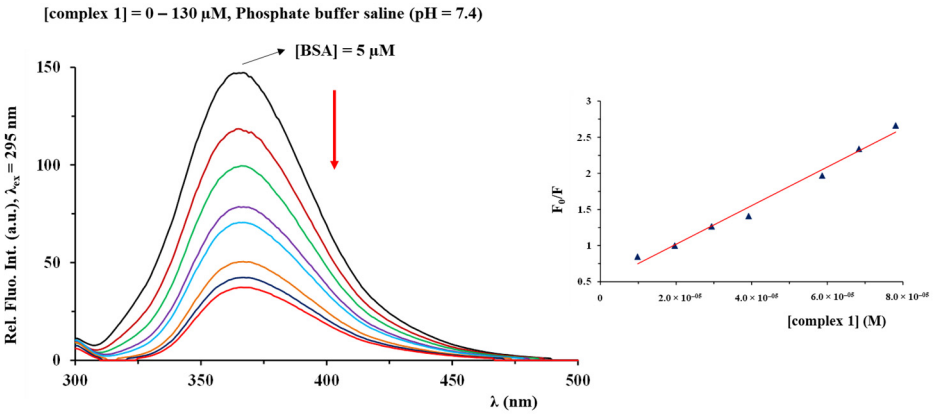

Figure 5. Fluorescence emission spectra of BSA in the presence of an increasing amount of complex **1**. The arrow shows the intensity changes upon increased concentration of the complex. Inserted graph: Stern-Volmer plots of F_0/F vs. complex.

The values of K_A constants indicate the ability of the complexes to bind to BSA and to be transported to their biological targets (Table 4) [50]. The number of binding sites per BSA molecule is 1.19 and 1.07 for **1** and **2**, respectively, suggesting their binding to only one binding site per protein molecule. The values of quenching constants K_q are higher than 10^{10} M^{-1} s^{-1}, indicating the static mechanism of BSA fluorescence quenching.

Table 4. Values of the binding constants of complexes **1** and **2** with BSA.

Complex	K_{sv} (M^{-1})	Hypochromism (%)	K_q (M^{-1} s^{-1})	K_A (M^{-1})	*n*
1	$(5.33 \pm 0.07) \times 10^4$	74.7	5.23×10^{12}	2.20×10^5	1.19
2	$(1.78 \pm 0.05) \times 10^4$	45.6	1.78×10^{12}	3.17×10^4	1.07

2.5.2. Synchronous Fluorescence Measurements

Synchronous fluorescence spectroscopy is a method that can be used to explore the structural changes in BSA in the presence of a metal complex [28]. This method was shown to be very useful for studying the microenvironment of amino acid residues by measuring the possible shift ($\Delta\lambda = \lambda_{em} - \lambda_{ex}$) in their maximum emission wavelength [51,52]. When $\Delta\lambda$ is 15 nm, the synchronous fluorescence is characteristic of the tyrosine (Tyr) residue, while a larger $\Delta\lambda$ value of 60 nm is due to tryptophan (Trp) [53].

The synchronous fluorescence spectra of BSA were recorded in the absence and presence of increasing amounts of investigated complexes **1** and **2**. As can be seen from Figure 6, a slight shift of the emission maxima was observed, indicating that the polarity of amino acid increases as a consequence of the interaction of the complex with BSA. Moreover, the fluorescence quenching constant of Tyr residue was slightly higher than that of Trp residue in the case of complex **1**, suggesting that Tyr residue contributes more to the fluorescence quenching (Table 5). The opposite is true for complex **2** (Table 5).

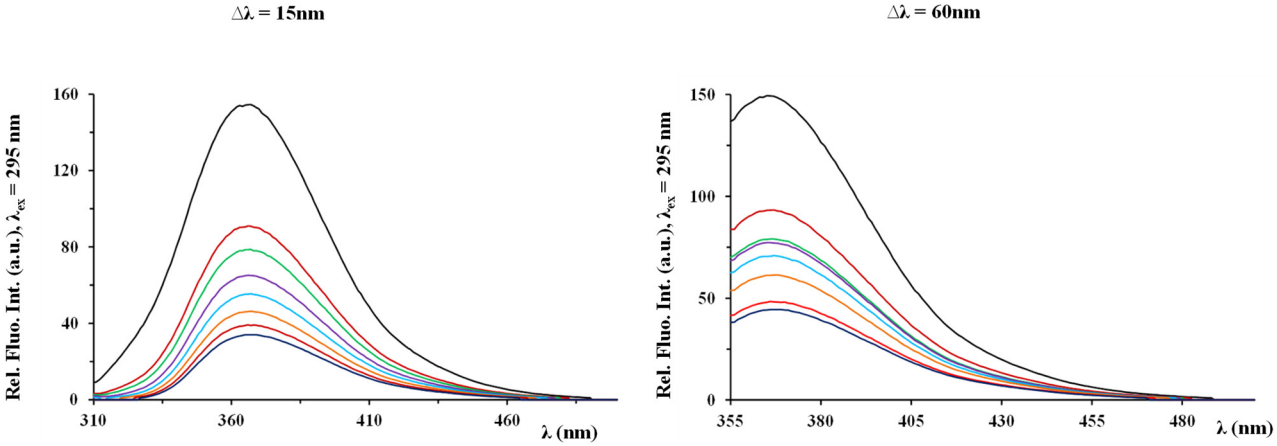

Figure 6. Synchronous fluorescence spectra of BSA in the absence and presence of increasing concentrations of complex **1** at Δλ = 15 and 60 nm.

Table 5. Values of the binding constants of complexes **1** and **2** with BSA obtained by synchronous fluorescence spectroscopy.

	Complex	K_{sv} (M^{-1})	Hypochromism (%)	K_q (M^{-1} s^{-1})	K_A (M^{-1})	n
Δλ = 15 nm	**1**	$(1.07 \pm 0.02) \times 10^6$	78.0	1.07×10^{14}	4.82×10^6	1.52
	2	$(3.23 \pm 0.01) \times 10^4$	67.2	3.23×10^{12}	2.90×10^5	1.30
Δλ = 60 nm	**1**	$(5.23 \pm 0.01) \times 10^4$	70.2	5.23×10^{12}	1.89×10^5	1.22
	2	$(4.39 \pm 0.01) \times 10^4$	70.1	4.39×10^{12}	6.90×10^5	1.38

3. Materials and Methods

3.1. Materials and Measurements

Zinc(II) chloride, zinc(II) bromide, ethanol, acetonitrile, dimethyl sulfoxide (DMSO), deuterated dimethyl sulfoxide (DMSO-d_6), phosphate buffer saline (PBS), calf thymus DNA (ct-DNA), ethidium bromide (EthBr) and bovine serum albumin (BSA) were purchased from the Sigma-Aldrich Chemical Co. All chemicals were of analytical grade and used without further purification. Solvents were used as received.

Elemental analyses of the synthesized zinc(II) complexes **1** and **2** for carbon, hydrogen, and nitrogen were done using a PerkinElmer 2400 Series II instrument (CHN). The IR spectra were recorded as KBr pellets on a PerkinElmer Spectrum One FT-IR spectrometer over the wavenumber range of 4000–450 cm^{-1}. The ^{1}H NMR spectra were recorded at room temperature on a Varian Gemini 2000 spectrometer at 200 MHz. 5.0 mg of a compound was dissolved in 0.6 mL of DMSO-d_6 and transferred into a 5 mm NMR tube. Chemical shifts, δ, are reported in ppm (parts per million), and scalar couplings, J, are reported in Hertz. Chemical shifts were calibrated relative to those of the solvent. The abbreviations for the peak multiplicities are the following: *s* (singlet), *d* (doublet), and *t* (triplet). The UV-Vis spectra were recorded on a Shimadzu double-beam spectrophotometer after dissolving the corresponding zinc(II) complex in DMSO, as well as after 24 and 48 h standing at ambient temperature, over the wavelength range of 900–200 nm. The concentration of the zinc(II) complexes was 8.6×10^{-5} and 4.9×10^{-5} M for **1** and **2**, respectively. Molar

conductivities were measured at room temperature on a digital conductivity-meter Crison Multimeter MM 41. The concentration of the solutions of complexes **1** and **2** in DMSO used for conductivity measurements was 1×10^{-3} M.

3.2. Synthesis of Dimethyl 2,2′-Bipyridine-4,5-dicarboxylate

Dimethyl 2,2′-bipyridine-4,5-dicarboxylate (py-2py) used for the synthesis of zinc(II) complexes was prepared by a previously published method [54]. The purity of this ligand was confirmed by elemental analysis and ^{1}H NMR spectroscopy.

3.3. Synthesis of Zinc(II) Complexes **1** *and* **2**

The solution of 1.0 mmol of py-2py ligand (272.3 mg) in 5.0 mL of ethanol was added slowly under stirring to the solution containing an equimolar amount of the zinc(II) salt (136.3 mg of $ZnCl_2$ for **1** and 225.2 mg of $ZnBr_2$ for **2**) in 5.0 mL of ethanol. The reaction mixture was stirred for 3 h at room temperature, and then, the precipitate was filtered off and recrystallized in 5.0 mL of acetonitrile. The obtained solutions were left at room temperature, and after 3–5 days, colorless crystals of complexes **1** and **2** were formed. These crystals were filtered off and dried at ambient temperature. Yield: 249.2 mg (61%) for **1** and 273.6 mg (55%) for **2**.

Anal. calcd for [Zn(py-2py)Cl_2] (**1**) = $C_{14}H_{12}ZnCl_2N_2O_4$ (MW = 408.53): C, 41.16; H, 2.96; N, 6.86. Found: C, 40.79; H, 2.79; N, 6.99%. IR (KBr, ν, cm^{-1}): 3123w, 3103w, 3067w, 3024w (ν(C_{ar}–H)), 2962w (ν(C–H)), 1742vs, 1724vs (ν(C=O)), 1616m, 1600m, 1572w, 1558m, 1497w, 1480w, 1441s, 1434s (ν(C_{ar}=C_{ar}) and ν(C_{ar}=N)), 1383s (ν_s(C=O)), 1318m, 1297m, 1277s, 1251m (ν(C–O)), 785m (γ(C_{ar}–H)). ^{1}H NMR (200 MHz, DMSO-d_6): δ = 3.91 (*t*, *J* = 3.0 Hz, 6H, Ar-$COOCH_3$), 7.62 (*d*, *J* = 0.9 Hz, 1H, H4′), 8.29 (*d*, *J* = 0.7, 1H, H5′), 8.48 (*d*, *J* = 7.8 Hz, 1H, H3′), 8.63 (*s*, 1H, H3), 9.05 (*d*, *J* = 0.7 Hz, 1H, H6), 9.14 (*s*, 1H, H6′) ppm. UV-Vis (DMSO, λ_{max}, nm): 306 ($\varepsilon = 9.1 \times 10^4$ M^{-1} cm^{-1}). Λ_M (DMSO): 5.0 Ω^{-1} cm^2 mol^{-1}.

Anal. calcd for [Zn(py-2py)Br_2] (**2**) = $C_{14}H_{12}ZnBr_2N_2O_4$ (MW = 497.45): C, 33.80; H, 2.43; N, 5.63. Found: C, 33.69; H, 2.52; N, 5.49%. IR (KBr, ν, cm^{-1}): 3123w, 3101w, 3066w (ν(C_{ar}–H)), 2960w, 2937w, (ν(C–H)), 1742vs, 1724vs (ν(C=O)), 1615m, 1599w, 1557w, 1495w, 1480w, 1440m, 1432w, (ν(C_{ar}=C_{ar}) and ν(C_{ar}=N)), 1382m (ν_s(C=O)), 1317m, 1296w, 1275s, 1250m (ν(C–O)), 784m (γ(C_{ar}–H)). ^{1}H NMR (200 MHz, DMSO-d_6): δ = 3.90 (*t*, *J* = 3.8 Hz, 6H, Ar-$COOCH_3$), 7.61 (*d*, *J* = 7.3 Hz, 1H, H4′), 8.27 (*s*, 1H, H5′), 8.51 (*d*, *J* = 7.3 Hz, 1H, H3′), 8.66 (*s*, 1H, H3), 9.03 (*s*, 1H, H6), 9.14 (*s*, 1H, H6′) ppm. UV-Vis (DMSO, λ_{max}, nm): 300 ($\varepsilon = 1.6 \times 10^4$ M^{-1} cm^{-1}). Λ_M (DMSO): 30.1 Ω^{-1} cm^2 mol^{-1}.

3.4. Crystallographic Data Collection and Refinement of the Structures

Data from single crystals **1** and **2** (Figure S8) were collected at 150 K on a SuperNova diffractometer with an Atlas detector using CrysAlis software (version 1.171.40.68a) with monochromated Mo Kα (0.71073 Å) [55]. The initial structural models were solved by direct methods implemented in SHELXT using the *Olex*2 graphical user interface [56]. A full-matrix least-squares refinement on F^2 magnitudes with anisotropic displacement parameters for all non-hydrogen atoms using *Olex*2 or *SHELXL*-2018/3 was employed [56,57]. All non-hydrogen atoms were refined anisotropically, while the hydrogen atoms were placed at calculated positions and treated as riding on their parent atoms. Additional details on the crystal data, data collection, and refinement are given in Table S1. Figures were prepared with *Mercury* [58]. CCDC 2162358 and 2162359 contain crystallographic data. These data can be obtained free of charge from The Cambridge Crystallographic Data Centre via www.ccdc.cam.ac.uk/data_request/cif (accessed on 14 April 2022).

3.5. Antimicrobial Studies

Zinc(II) complexes **1** and **2** were tested in multiple biological assays to determine whether they have antimicrobial activity. The corresponding inorganic salts, $ZnCl_2$ and $ZnBr_2$, and py-2py ligand, used as starting compounds in the synthesis of complexes, were also included in the bioactivity assessment.

3.5.1. Determination of Minimum Inhibitory Concentration (MIC) on Bacterial and Fungal Strains

A standardized methodology for the determination of MIC values used in this study is recommended by the National Committee for Clinical Laboratory Standards (M07-A8) for bacteria and Standards of the European Committee on Antimicrobial Susceptibility Testing (v 7.3.1: Method for the determination of broth dilution minimum inhibitory concentrations of antifungal agents for yeasts) for *Candida* spp. [59]. For the assessment of the antimicrobial potential of complexes **1** and **2**, two bacterial (*P. aeruginosa* NCTC 10332 and *S. aureus* ATCC 25923) and two fungal strains (*C. albicans* ATCC 10231 and *C. parapsilosis* ATCC 22019) were used. All tested complexes and salts were firstly dissolved in DMSO, at a concentration of 50 mg/mL. The highest concentration tested for the antimicrobial activity was 500 μg/mL. The inoculums were 5×10^5 colony-forming units, cfu/mL for bacteria and 1×10^5 cfu/mL for fungal species. The MIC value was recorded as the lowest concentration that inhibited the growth after 24 h at 37 °C, using the Tecan Infinite 200 Pro multiplate reader (Tecan Group Ltd., Männedorf, Switzerland).

3.5.2. Inhibition of Quorum Sensing Signaling Pathways, Testing Compounds Impact on the Production of Violacein and Prodigiosin Pigments

For the assessment of the violacein production, the *Chromobacterium violaceum* CV026 biosensor strain was used [60]. This strain was cultivated in an LB growth medium supplemented with appropriate antibiotics overnight at 30 °C and 180 rpm on a rotary shaker. Into semi-solid LB agar (0.3%, *w*/*v*, 5 mL), 50 μL of an overnight culture of *C. violaceum* CV026 supplemented with *N*-hexanoyl-L-homoserine lactone (Sigma, Steinheim, Germany) to a final concentration of 5 μM was seeded and poured over the surface of LB agar plates. After solidification, the sterile discs were placed on the surface of plates, and complexes were added in appropriate concentrations (500 and 250 μg per disc). Petri dishes were incubated at 30 °C in an upright position overnight.

Serratia marcescens ATCC 27117 was used for the assessment of prodigiosin production. The methodology was the same as for the *C. violaceum* CV026 assay besides adding an external autoinducer because this is a wild-type strain naturally capable of its production [61]. Inhibition of violacein and prodigiosin production was defined as the presence of blurry white hallows around discs containing active compounds, measured in mm, and was distinguished from the zones of clearance that indicated inhibition of growth of the tested strains.

3.5.3. *C. albicans* ATCC 10231 Hyphae Formation

The effect of complexes **1** and **2** on *C. albicans* ATCC 10231 hyphae formation was assessed using two growth media, solid Spider [36] and RPMI (Roswell Park Memorial Institute Medium) broth (Sigma-Aldrich, Munich, Germany). On Spider medium, the formation of *C. albicans* ATCC 10231 hyphae was monitored for 72 h, in the presence of complexes in subinhibitory concentrations, 50 and 25 μg/mL. The growth was observed and photographed under a stereomicroscope (SMZ143-N2GG, Motic, Wetzlar, Germany). Additionally, hyphae formation was studied in a liquid RPMI medium supplemented with 2% (*v*/*w*) glucose. The *C. albicans* ATCC 10231 cells (firstly grown in Sabouraud dextrose broth medium at 30 °C overnight and washed with sterile PBS, phosphate-buffered saline) were seeded to the final concentration of 1×10^6 cells/mL. Cell suspension was treated with 0.5 × MIC concentrations of both complexes for 3 h at 37 °C with shaking at 180 rpm on a rotary shaker. The cells treated with DMSO were used as control. Finally, cells were pelleted at 3000 g, concentrated 10 times in fresh PBS, smeared on the glass slide, heat fixed, and stained with Loffler's alkaline methylene blue solution (HiMedia Laboratories, Mumbai, India), and the hyphae formation was observed using bright field microscopy (Olympus BX51, Applied Imaging Corp., San Jose, CA, USA) under 20 × magnification.

3.5.4. Inhibition of *C. albicans* ATCC 10231 Biofilm Formation

The biofilm formation of *C. albicans* ATCC 10231 was tested in the presence of zinc(II) complexes **1** and **2**, using the previously described methodology [37] with some minor modifications. Starting inoculums for the biofilm inhibition assay was 1×10^6 cfu/mL and the concentration gradient of the tested complexes was from 125 µg/mL with twofold serial dilutions following up to 3.9 µg/mL. The lowest concentration that inhibited biofilm formation was evaluated after incubation for 48 h at 37 °C. Biofilm growth was quantified by crystal violet (CV) staining of adherent cells and estimated as absorbance at 590 nm on Tecan Infinite 200 Pro multiplate reader (Tecan Group Ltd., Männedorf, Switzerland). The assay was repeated three times to achieve low standard deviations.

3.6. In Vitro Toxicity

Antiproliferative activity of the complexes **1** and **2**, the corresponding zinc(II) salts, and py-2py was determined by 3-(4,5-dimethylthiazol-2-yl)-2,5-diphenyltetrazolium bromide (MTT) assay [62] on human lung fibroblasts cells MRC-5, obtained from the American Type Culture Collection (ATCC). The inoculums of 1×10^4 cells per well were cultured in the complete RPMI 1640 medium (Gibco™ by Thermo Fischer Scientific, CE) as a monolayer and further incubated with the tested compounds at a concentration from a maximum of 120 µM, in a humidified atmosphere of 95% air and 5% CO_2 at 37 °C for 48 h. The extent of MTT reduction was measured spectrophotometrically at 540 nm using a Tecan Infinite 200 Pro multiplate reader (Tecan Group Ltd., Männedorf, Switzerland). Cytotoxicity was expressed as the concentration of the complex inhibiting cell growth by 50% (IC_{50}) in comparison with the negative control (DMSO-treated cells).

3.7. Survival Assay on In Vivo Model Organism Caenorhabditis Elegans

The nematode *C. elegans* AU37, obtained from the Caenorhabditis Genetics Center (CGC), University of Minnesota, Minneapolis, MN, USA. *C. elegans* AU37 (glp-4; sek-1), was used to establish the toxicity of complexes **1** and **2**. The worm was propagated under standard conditions, synchronized by hypochlorite bleaching, and cultured on a nematode growth medium using *E. coli* OP50 as a food source, as described previously [63]. The *C. elegans* AU37 survival assay was carried out following the standard procedure [64] with some minor modifications. Briefly, synchronized worms (L4 stage) were suspended in a medium containing 95% M9 buffer (3.0 g of KH_2PO_4, 6.0 g of Na_2HPO_4, 5.0 g of NaCl, and 1 mL of 1 M $MgSO_4 \cdot 7H_2O$ in 1 L of water), 5% LB broth (Oxoid, Basingstoke, UK), and 10 µg/mL of cholesterol (Sigma-Aldrich, Munich, Germany). The experiment was carried out in 96-well flat-bottomed microtiter plates (Sarstedt, Nümbrecht, Germany) with a final volume of 100 µL per well. The wells were filled with 50 µL of the medium, 25 µL of the suspension of nematodes (25–35 nematodes), and 25 µL of the solvent control (1% DMSO) or 25 µL of the concentrated tested compound solution (complexes at appropriate concentrations). Final concentrations of the complexes were 500, 200, 100, 50, 10 µg/mL. Subsequently, the plates were incubated at 25 °C for three days. The fraction of dead worms was determined after 48 and 72 h by counting the number of dead worms and the total number of worms in each well, using a stereomicroscope (SMZ143-N2GG, Motic, Germany). The compounds were tested three times in each assay, and each assay was repeated two times ($n = 6$). As a negative control experiment, nematodes were exposed to the medium containing 1% DMSO.

3.8. DNA Interaction

The DNA interaction study was carried out in PBS buffer (pH = 7.4) by maintaining [ct-DNA]/[EthBr] = 5, while increasing the concentration of the complexes **1** and **2**. Each sample solution was scanned in the wavelength range of 525–750 nm at an excitation wavelength of 520 nm. The Stern–Volmer constants (K_{sv}) were calculated using the following equation [44]:

$$F_0/F = 1 + K_q\tau_0[\text{complex}] = 1 + K_{sv}[\text{complex}]$$

where F_0 and F are the fluorescence intensities in the absence and presence of the complexes, respectively. K_q stands for bimolecular quenching constant and τ_0 (10^{-8} s) is the lifetime of the fluorophore in the absence of the quencher. The binding constants (K_A) and apparent binding sites (n) can be calculated by using the following equation [65]:

$$\log(F_0 - F)/F = \log K_A + n \log[\text{complex}]$$

where K_A stands for the binding constant of the zinc(II) complex with ct-DNA, and n stands for the apparent number of binding sites.

DNA interaction assay using gel electrophoresis was performed according to the previously published methodology [66] with commercial lambda bacteriophage DNA (300 ng, Thermo Scientific™, Waltham, MA, USA). The final DNA concentration of 20 ng/µL was incubated with 500 µg/mL of complexes **1** and **2** at 37 °C. After incubation 300 ng per lane of samples were run on 0.8% agarose gel with EthBr against a HyperLadder™ 1 kb DNA Ladder plus (FastGene) at 60 V for 1 h. Gels were visualized and analyzed using the Biometra Gel Imaging system (Biometra, Gottingen, Germany) equipped with the BioDocAnalyze 2.2 Software.

3.9. Protein Binding Study

The protein binding study was performed by tryptophan fluorescence quenching experiments using BSA (5.0 µM) in PBS (pH = 7.4). The quenching of the emission intensity of the tryptophan residues of bovine serum albumin (BSA) at 367 nm was monitored at increasing concentrations of complexes **1** and **2** (up to 130 µM). The fluorescence spectra were recorded in the range of 300–500 nm with an excitation wavelength of 295 nm. The corresponding binding constants of the complexes (K_A) and apparent binding sites (n) were calculated as it was above explained [46,65]. For the synchronous fluorescence spectroscopy studies, the same concentration of BSA and complexes **1** and **2** was used, and the spectra were measured at two different $\Delta\lambda$ values ($\Delta\lambda = \lambda_{em} - \lambda_{ex}$), 15 and 60 nm, which are characteristic of the tyrosine (Tyr) and tryptophan (Trp) residues, respectively.

4. Conclusions

In this study, two new zinc(II) complexes with dimethyl 2,2′-bipyridine-4,5-dicarboxylate (py-2py), [Zn(py-2py)Cl_2] (**1**) and [Zn(py-2py)Br_2] (**2**), were synthesized, structurally characterized, and biologically evaluated. Reactions of py-2py with ZnX_2 salt (X is Cl^- or Br^-) lead to the formation of isostructural complexes **1** and **2**, which adopt a slightly distorted tetrahedral geometry. The nature of the coordinated halogenido ligand in these complexes was reflected in slight differences in their biological activities. Thus, complex **1** was the only one that showed moderate antimicrobial activity against the *Candida* strains studied, whereas complex **2**, as well as the other compounds studied (both zinc(II) salts and the free py-2py ligand), showed neither antibacterial nor antifungal activity. Also, the cytotoxicity of complex **1** against healthy fibroblasts was twice that of complex **2**, but neither complex had any in vivo effect on the survival rate of *C. elegans*. While complex **2** was more effective in inhibiting hyphae formation, its structural analog **1** showed a better ability in preventing biofilm formation. Both inhibitions of filamentation of *C. albicans* and biofilm formation are highly desirable properties of a novel antimicrobial agent. Complex **1** also showed moderate activity for the quorum sensing inhibitory potential on two investigated biosensor strains. This can be of importance for the development of novel anti-virulence therapeutic agents that attenuate virulence without a pronounced effect on bacterial growth, thus offering a lower risk for resistance development. The different binding affinity of the complexes **1** and **2** toward DNA may result from difference in the nature of halogenido ligands and easier hydrolysis of Zn–Br with respect to the Zn–Cl bond, which could be due to a hard character of Zn(II) ion and soft character of bromide, while chloride behaves as an intermediate ion.

Supplementary Materials: The following supporting information can be downloaded at: https://www.mdpi.com/article/10.3390/inorganics10060071/s1, Figure S1: C_{Ar}–H···Cl and C_{Ar}–H···Br interactions in complexes **1** and **2**. Selected distances (Å): (**1**) H6′′-Cl1 2.761, H11-Cl2′ 2.875, H12-Cl2′′ 2.855, (**2**) H6′′-Br2 2.851, H11-Br1′ 3.010, H12-Br1′′ 2.941; Figure S2: ^{1}H NMR spectrum of complex **1** recorded in DMSO-d_6 at room temperature; Figure S3: Time stability of complex **2** followed by UV-Vis spectrophotometry at room temperature in DMSO; Figure S4: *C. elegans* under the microscope after 72 h of incubation with complexes **1** and **2** and the corresponding zinc(II) salts; Figure S5: Filamentation of *C. albicans* ATCC 10231 in the presence of zinc(II) complex **2** (25 μg/mL), $ZnBr_2$ (25 μg/mL) and amphotericin B (1 μg/mL) in RPMI liquid medium (Olympus BX51, Applied Imaging Corp., San Jose, CA, United States, under 20 × magnification); Figure S6: Inhibition of prodigiosin (a) and violacein (b) production in the presence of zinc(II) complexes **1** and **2**, and the corresponding zinc(II) salts tested on *Serratia marcescens* (a) and *Chromobacterium violaceum* CV026 (b) at 500 μg per disc concentration; Figure S7: Fluorescence emission spectra of EthBr–DNA system in the presence of an increasing amount of complexes **1** (a) and **2** (b). The arrow shows the intensity changes upon the gradual addition of the complex. Inserted graph: Stern-Volmer plots of F_0/F vs. complex; Figure S8: Photographs of single crystals of complexes **1** and **2**; Table S1: Details of the crystal structure determination for complexes **1** and **2**; Experimental data for dimethyl 2,2′-bipyridine-4,5-dicarboxylate (py-2py).

Author Contributions: Conceptualization, T.P.A., I.T., M.I.D. and B.Đ.G.; methodology, T.P.A., I.A., J.K., B.V.P., D.M. and S.V.; software, J.K.; validation, I.T., M.I.D. and B.Đ.G.; investigation, T.P.A., I.A., J.K., B.V.P., D.M. and S.V.; resources, I.T. and M.I.D.; writing—original draft preparation, T.P.A., I.A., J.K., B.V.P., D.M. and S.V.; writing—review and editing, I.T., M.I.D. and B.Đ.G.; visualization, T.P.A., I.A., J.K., B.V.P., D.M. and S.V.; supervision, I.T., M.I.D. and B.Đ.G. All authors have read and agreed to the published version of the manuscript.

Funding: This research has been financially supported by the Ministry of Education, Science and Technological Development of the Republic of Serbia (Agreements No. 451-03-68/2022-14/200042 and 451-03-68/2022-14/200122) and by the Slovenian Research Agency (grant P1-0175). The EN→FIST Centre of Excellence, Trg OF 13, SI-1000 Ljubljana, Slovenia, is acknowledged for the use of the SuperNova diffractometer. This research has also received funding from the Serbian Academy of Sciences and Arts under project No. F128.

Data Availability Statement: The spectroscopic data used to support the findings of this study are available on request from the corresponding authors.

Conflicts of Interest: The authors declare no conflict of interest. The funders had no role in the design of the study; in the collection, analyses, or interpretation of data; in the writing of the manuscript, or in the decision to publish the results.

References

1. Osredkar, J.; Sustar, N. Copper and Zinc, Biological Role and Significance of Copper/Zinc Imbalance. *J. Clin. Toxicol.* **2011**, *S3*, 495. [CrossRef]
2. Krężel, A.; Maret, W. The biological inorganic chemistry of zinc ions. *Arch. Biochem. Biophys.* **2016**, *611*, 3–19. [CrossRef] [PubMed]
3. Myari, A.; Malandrinos, G.; Deligiannakis, Y.; Plakatouras, J.C.; Hadjiliadis, N.; Nagy, Z.; Sòvágó, I. Interaction of Cu^{2+} with His–Val–His and of Zn^{2+} with His–Val–Gly–Asp, two peptides surrounding metal ions in Cu,Zn-superoxide dismutase enzyme. *J. Inorg. Biochem.* **2001**, *85*, 253–261. [CrossRef]
4. Krishnamurthy, V.M.; Kaufman, G.K.; Urbach, A.R.; Gitlin, I.; Gudiksen, K.L.; Weibel, D.B.; Whitesides, G.M. Carbonic anhydrase as a model for biophysical and physical-organic studies of proteins and protein-ligand binding. *Chem. Rev.* **2008**, *108*, 946–1051. [CrossRef] [PubMed]
5. Haase, H.; Rink, L. Multiple impacts of zinc on immune function. *Metallomics* **2014**, *6*, 1175–1180. [CrossRef]
6. Kolenko, V.; Teper, E.; Kutikov, A.; Uzzo, R. Zinc and zinc transporters in prostate carcinogenesis. *Nat. Rev. Urol.* **2013**, *10*, 219–226. [CrossRef] [PubMed]
7. Walkup, G.K.; Burdette, S.C.; Lippard, S.J.; Tsien, R.Y. A new cell-permeable fluorescent probe for Zn^{2+}. *J. Am. Chem. Soc.* **2000**, *122*, 5644–5645. [CrossRef]
8. Pellei, M.; Del Bello, F.; Porchia, M.; Santini, C. Zinc coordination complexes as anticancer agents. *Coord. Chem. Rev.* **2021**, *445*, 214088. [CrossRef]
9. Michalczyk, K.; Cymbaluk-Płoska, A. The role of zinc and copper in gynecological malignancies. *Nutrients* **2020**, *12*, 3732. [CrossRef]
10. Murakami, M.; Hirano, T. Intracellular zinc homeostasis and zinc signaling. *Cancer Sci.* **2008**, *99*, 1515–1522. [CrossRef]

11. Li, Y.V. Zinc and insulin in pancreatic beta-cells. *Endocrine* **2014**, *45*, 178–189. [CrossRef] [PubMed]
12. Taylor, C.G. Zinc, the pancreas, and diabetes: Insights from rodent studies and future directions. *Biometals* **2005**, *18*, 305–312. [CrossRef] [PubMed]
13. Bjørklund, G.; Dadar, M.; Pivina, L.; Doşa, M.D.; Semenova, Y.; Aaseth, J. The role of zinc and copper in insulin resistance and diabetes mellitus. *Curr. Med. Chem.* **2020**, *27*, 6643–6657. [CrossRef] [PubMed]
14. Szunyogová, E.; Mudroňová, D.; Györyová, K.; Nemcová, R.; Kovářová, J.; Piknová-Findoráková, L. The physicochemical and biological properties of zinc(II) complexes. *J. Therm. Anal. Calorim.* **2007**, *88*, 355–361. [CrossRef]
15. Cuajungco, M.P.; Ramirez, M.S.; Tolmasky, M.E. Zinc: Multidimensional effects on living organisms. *Biomedicines* **2021**, *9*, 208. [CrossRef] [PubMed]
16. Ye, Q.; Chen, W.; Huang, H.; Tang, Y.; Wang, W.; Meng, F.; Wang, H.; Zheng, Y. Iron and zinc ions, potent weapons against multidrug-resistant bacteria. *Appl. Microbiol. Biotechnol.* **2020**, *104*, 5213–5227. [CrossRef]
17. Abendrot, M.; Kalinowska-Lis, U. Zinc-containing compounds for personal care applications. *Int. J. Cosmet. Sci.* **2018**, *40*, 319–327. [CrossRef]
18. Sánchez-López, E.; Gomes, D.; Esteruelas, G.; Bonilla, L.; Lopez-Machado, A.L.; Galindo, R.; Cano, A.; Espina, M.; Ettcheto, M.; Camins, A.; et al. Metal-based nanoparticles as antimicrobial agents: An overview. *Nanomaterials* **2020**, *10*, 292. [CrossRef]
19. Raghupathi, K.R.; Koodali, R.T.; Manna, A.C. Size-dependent bacterial growth inhibition and mechanism of antibacterial activity of zinc oxide nanoparticles. *Langmuir* **2011**, *27*, 4020–4028. [CrossRef]
20. Liang, J.; Sun, D.; Yang, Y.; Li, M.; Li, H.; Chen, L. Discovery of metal-based complexes as promising antimicrobial agents. *Eur. J. Med. Chem.* **2021**, *224*, 113696. [CrossRef]
21. Gupta, M.; Mahajan, V.K.; Mehta, K.S.; Chauhan, P.S. Zinc therapy in dermatology: A review. *Dermatol. Res. Pract.* **2014**, *2014*, 709152. [CrossRef] [PubMed]
22. Pittol, M.; Tomachesk, D.; Simões, D.N.; Ribeiro, V.F.; Santana, R.M.C. Antimicrobial performance of thermoplastic elastomers containing zinc pyrithione and silver nanoparticles. *Mater. Res.* **2017**, *20*, 1266–1273. [CrossRef]
23. Kalinowska, M.; Sienkiewicz-Gromiuk, J.; Świderski, G.; Pietryczuk, A.; Cudowski, A.; Lewandowski, W. Zn(II) complex of plant phenolic chlorogenic acid: Antioxidant, antimicrobial and structural studies. *Materials* **2020**, *13*, 3745. [CrossRef] [PubMed]
24. Kalinowska, M.; Piekut, J.; Bruss, A.; Follet, C.; Sienkiewicz-Gromiuk, J.; Świsłocka, R.; Rzączyńska, Z.; Lewandowski, W. Spectroscopic (FT-IR, FT-Raman, ^{1}H, ^{13}C NMR, UV/VIS), thermogravimetric and antimicrobial studies of Ca(II), Mn(II), Cu(II), Zn(II) and Cd(II) complexes of ferulic acid. *Spectrochim. Acta A Mol. Biomol. Spectrosc.* **2014**, *122*, 631–638. [CrossRef] [PubMed]
25. Andrejević, T.P.; Warżajtis, B.; Glišić, B.Đ.; Vojnovic, S.; Mojicevic, M.; Stevanović, N.L.; Nikodinovic-Runic, J.; Rychlewska, U.; Djuran, M.I. Zinc(II) complexes with aromatic nitrogen-containing heterocycles as antifungal agents: Synergistic activity with clinically used drug nystatin. *J. Inorg. Biochem.* **2020**, *208*, 111089. [CrossRef] [PubMed]
26. McCall, K.A.; Huang, C.; Fierke, C.A. Zinc and SARS-CoV-2: A molecular modeling study of Zn interactions with RNA-dependent RNA-polymerase and 3C-like proteinase enzymes. *Int. J. Mol. Med.* **2021**, *47*, 326–334.
27. Andrejević, T.P.; Milivojevic, D.; Glišić, B.Đ.; Kljun, J.; Stevanović, N.L.; Vojnovic, S.; Medic, S.; Nikodinovic-Runic, J.; Turel, I.; Djuran, M.I. Silver(I) complexes with different pyridine-4,5-dicarboxylate ligands as efficient agents for the control of cow mastitis associated pathogens. *Dalton Trans.* **2020**, *49*, 6084–6096. [CrossRef]
28. Andrejević, T.P.; Aleksic, I.; Počkaj, M.; Kljun, J.; Milivojevic, D.; Stevanović, N.L.; Nikodinovic-Runic, J.; Turel, I.; Djuran, M.I.; Glišić, B.Đ. Tailoring copper(II) complexes with pyridine-4,5-dicarboxylate esters for anti-*Candida* activity. *Dalton Trans.* **2021**, *50*, 2627–2638. [CrossRef]
29. Traven, K.; Eleftheriadis, N.; Seršen, S.; Kljun, J.; Bezenšek, J.; Stanovnik, B.; Turel, I.; Dekker, F.J. Ruthenium complexes as inhibitors of 15-lipoxygenase-1. *Polyhedron* **2015**, *101*, 306–313. [CrossRef]
30. Traven, K.; Sinreih, M.; Stojan, J.; Seršen, S.; Kljun, J.; Bezenšek, J.; Stanovnik, B.; Turel, I.; Lanišnik Rižner, T. Ruthenium complexes as inhibitors of the aldo–keto reductases AKR1C1–1C3. *Chem.-Biol. Interact.* **2015**, *234*, 349–359. [CrossRef]
31. Traven, K.; Turel, I.; Koziskova, J.; Bučinský, L.; Kozisek, J. Concomitant polymorphism in an organometallic ruthenium(II) complex with an *N*,*N*′-donor ligand. *Acta Crystallogr. C Struct. Chem.* **2018**, *74*, 683–689. [CrossRef] [PubMed]
32. Yang, L.; Powella, D.R.; Houser, R.P. Structural variation in copper(I) complexes with pyridylmethylamide ligands: Structural analysis with a new four-coordinate geometry index, τ4. *Dalton Trans.* **2007**, 955–964. [CrossRef]
33. Okuniewski, A.; Rosiak, D.; Chojnacki, J.; Becker, B. Coordination polymers and molecular structures among complexes of mercury(II) halides with selected 1-benzoylthioureas. *Polyhedron* **2015**, *90*, 47–57. [CrossRef]
34. Rosiak, D.; Okuniewski, A.; Chojnacki, J. Novel complexes possessing Hg–(Cl, Br, I)···O=C halogen bonding and unusual $Hg_2S_2(Br/I)_4$ kernel. The usefulness of τ4′ structural parameter. *Polyhedron* **2018**, *146*, 35–41. [CrossRef]
35. Geary, W.J. The use of conductivity measurements in organic solvents for the characterisation of coordination compounds. *Coord. Chem. Rev.* **1971**, *7*, 81–122. [CrossRef]
36. Liu, H.; Köhler, J.; Fink, G.R. Suppression of hyphal formation in *Candida albicans* by mutation of a STE12 homolog. *Science* **1994**, *266*, 1723–1726. [CrossRef]
37. Pierce, C.G.; Uppuluri, P.; Tristan, A.R.; Wormley, F.L., Jr.; Mowat, E.; Ramage, G.; Lopez-Ribot, J.L. A simple and reproducible 96-well plate-based method for the formation of fungal biofilms and its application to antifungal susceptibility testing. *Nat. Protoc.* **2008**, *3*, 1494–1500. [CrossRef]

38. Stevanović, N.L.; Aleksic, I.; Kljun, J.; Bogojevic, S.S.; Veselinovic, A.; Nikodinovic-Runic, J.; Turel, I.; Djuran, M.I.; Glišić, B.Đ. Copper(II) and Zinc(II) complexes with the clinically used fluconazole: Comparison of antifungal activity and therapeutic potential. *Pharmaceuticals* **2021**, *14*, 24. [CrossRef]
39. López-Ribot, J.L. *Candida albicans* biofilms: More than filamentation. *Curr. Biol.* **2005**, *15*, R453–R455. [CrossRef]
40. Krzyżek, P. Challenges and limitations of anti-quorum sensing therapies. *Front. Microbiol.* **2019**, *10*, 2473. [CrossRef]
41. Chen, X.; Zhang, L.; Zhang, M.; Liu, H.; Lu, P.; Lin, K. Quorum sensing inhibitors: A patent review (2014–2018). *Expert Opin. Ther. Pat.* **2018**, *28*, 849–865. [CrossRef] [PubMed]
42. Stevanović, N.L.; Kljun, J.; Aleksic, I.; Bogojevic, S.S.; Milivojevic, D.; Veselinovic, A.; Turel, I.; Djuran, M.I.; Nikodinovic-Runic, J.; Glišić, B.Đ. Clinically used antifungal azoles as ligands for gold(III) complexes: The influence of the Au(III) ion on the antimicrobial activity of the complex. *Dalton Trans.* **2022**, *51*, 5322–5334. [CrossRef] [PubMed]
43. Lakowicz, J.R. *Principles of Fluorescence Spectroscopy*, 3rd ed.; Plenum Press: New York, NY, USA, 2006.
44. Smoleński, P.; Pettinari, C.; Marchetti, F.; da Silva, M.F.C.G.; Lupidi, G.; Patzmay, G.V.B.; Petrelli, D.; Vitali, L.A.; Pomberio, A.J.L. Syntheses, structures, and antimicrobial activity of new remarkably light-stable and water-soluble tris(pyrazolyl)methanesulfonate silver(I) derivatives of N-methyl-1,3,5-triaza-7-phosphaadamantane salt—[mPTA]BF4. *Inorg. Chem.* **2015**, *54*, 434–440. [CrossRef] [PubMed]
45. Pavic, A.; Savić, N.D.; Glišić, B.Đ.; Crochet, A.; Vojnovic, S.; Kurutos, A.; Stanković, D.M.; Fromm, K.M.; Nikodinovic-Runic, J.; Djuran, M.I. Silver(I) complexes with 4,7-phenanthroline efficient in rescuing the zebrafish embryos of lethal *Candida albicans* infection. *J. Inorg. Biochem.* **2019**, *195*, 149–163. [CrossRef]
46. Shi, Y.; Guo, C.; Sun, Y.; Liu, Z.; Xu, F.; Zhang, Y.; Wen, Z.; Li, Z. Interaction between DNA and microcystin-LR studied by spectra analysis and atomic force microscopy. *Biomacromolecules* **2011**, *12*, 797–803. [CrossRef] [PubMed]
47. Pearson, R.G. Hard and soft acids and bases—The evolution of a chemical concept. *Coord. Chem. Rev.* **1990**, *100*, 403–425. [CrossRef]
48. Wu, H.-L.; Li, W.-Y.; He, X.-W.; Miao, K.; Liang, H. Spectral studies of the binding of lucigenin, a bisacridinium derivative, with double-helix DNA. *Anal. Bioanal. Chem.* **2002**, *373*, 163–168. [CrossRef]
49. Tarushi, A.; Totta, X.; Papadopoulos, A.; Kljun, J.; Turel, I.; Kessissoglou, D.P.; Psomas, G. Antioxidant activity and interaction with DNA and albumins of zinc–tolfenamato complexes. Crystal structure of [Zn(tolfenamato)$_2$(2,2′-dipyridylketoneoxime)$_2$]. *Eur. J. Med. Chem.* **2014**, *74*, 187–198. [CrossRef]
50. Rajendiran, V.; Karthik, R.; Palaniandavar, M.; Stoeckli-Evans, H.; Periasamy, V.S.; Akbarsha, M.A.; Srinag, B.S.; Krishnamurthy, H. Mixed-ligand copper(II)-phenolate complexes: effect of coligand on enhanced DNA and protein binding, DNA cleavage, and anticancer activity. *Inorg. Chem.* **2007**, *46*, 8208–8221. [CrossRef]
51. Li, D.; Zhu, M.; Xu, C.; Ji, B. Characterization of the baicalein–bovine serum albumin complex without or with Cu^{2+} or Fe^{3+} by spectroscopic approaches. *Eur. J. Med. Chem.* **2011**, *46*, 588–599. [CrossRef]
52. Hemmateenejad, B.; Shamsipur, M.; Samari, F.; Khayamian, T.; Ebrahimi, M.; Rezaei, Z. Combined fluorescence spectroscopy and molecular modeling studies on the interaction between harmalol and human serum albumin. *J. Pharm. Biomed. Anal.* **2012**, *67*, 201–208. [CrossRef] [PubMed]
53. Da Silva, J.G.; Recio Despaigne, A.A.; Louro, S.R.W.; Bandeira, C.C.; Souza-Fagundes, E.M.; Beraldo, H. Cytotoxic activity, albumin and DNA binding of new copper(II) complexes with chalcone-derived thiosemicarbazones. *Eur. J. Med. Chem.* **2013**, *65*, 415–426. [CrossRef] [PubMed]
54. Bezenšek, J.; Prek, B.; Grošelj, U.; Kasunič, M.; Svete, J.; Stanovnik, B. A simple metal-free synthesis of 2-substituted pyridine-4,5-dicarboxylates and their *N*-oxides. *Tetrahedron* **2012**, *68*, 4719–4731. [CrossRef]
55. Oxford Diffraction Ltd. *CrysAlis PRO*; Agilent Technologies: Yarnton, UK, 2011.
56. Dolomanov, O.V.; Bourhis, L.J.; Gildea, R.J.; Howard, J.A.K.; Puschmann, H. *OLEX2*: A complete structure solution, refinement and analysis program. *J. Appl. Crystallogr.* **2009**, *42*, 339–341. [CrossRef]
57. Sheldrick, G.M. *Shelxl 2018/3*; University of Göttingen: Göttingen, Germany, 2018.
58. Macrae, C.F.; Edgington, P.R.; McCabe, P.; Pidcock, E.; Shields, G.P.; Taylor, R.; Towler, M.; van de Streek, J. *Mercury*: Visualization and analysis of crystal structures. *J. Appl. Crystallogr.* **2006**, *49*, 453–457. [CrossRef]
59. Arendrup, M.C.; Cuenca-Estrella, M.; Lass-Flörl, C.; Hope, W. the EUCAST-AFST. EUCAST technical note on the EUCAST definitive document EDef 7.2: Method for the determination of broth dilution minimum inhibitory concentrations of antifungal agents for yeasts EDef 7.2 (EUCAST-AFST). *Clin. Microbiol. Infect.* **2012**, *18*, E246–E247. [CrossRef]
60. McClean, K.H.; Winson, M.K.; Fish, L.; Taylor, A.; Chhabra, S.R.; Camara, M.; Daykin, M.; Lamb, J.H.; Swift, S.; Bycroft, B.W.; et al. Quorum sensing and *Chromobacterium violaceum*: Exploitation of violacein production and inhibition for the detection of *N*-acylhomoserine lactones. *Microbiology* **1997**, *143*, 3703–3711. [CrossRef]
61. Aleksić, I.; Šegan, S.; Andrić, F.; Zlatović, M.; Moric, I.; Opsenica, D.M.; Senerovic, L. Long-chain 4-aminoquinolines as quorum sensing inhibitors in *Serratia marcescens* and *Pseudomonas aeruginosa*. *ACS Chem. Biol.* **2017**, *12*, 1425–1434. [CrossRef]
62. Ferrer, F.; Fanciullino, R.; Milano, G.; Ciccolini, J. Towards rational cancer therapeutics: Optimizing dosing, delivery, scheduling, and combinations. *Clin. Pharmacol. Ther.* **2020**, *108*, 458–470. [CrossRef]
63. Stiernagle, T. *Maintenance of C. elegans*; The *C. elegans* Research Community, Ed.; WormBook: Minneapolis, MN, USA, 2006.

64. Brackman, G.; Cos, P.; Maes, L.; Nelis, H.J.; Coenye, T. Quorum sensing inhibitors increase the susceptibility of bacterial biofilms to antibiotics in vitro and in vivo. *Antimicrob. Agents Chemother.* **2011**, *55*, 2655–2661. [CrossRef]
65. Wolfe, A.; Shimer, G.H., Jr.; Meehan, T. Polycyclic aromatic hydrocarbons physically intercalate into duplex regions of denatured DNA. *Biochemistry* **1987**, *26*, 6392–6396. [CrossRef] [PubMed]
66. Savić, N.D.; Vojnovic, S.; Glišić, B.Đ.; Crochet, A.; Pavic, A.; Janjić, G.V.; Pekmezović, M.; Opsenica, I.M.; Fromm, K.M.; Nikodinovic-Runic, J.; et al. Mononuclear silver(I) complexes with 1,7-phenanthroline as potent inhibitors of *Candida* growth. *Eur. J. Med. Chem.* **2018**, *156*, 760–773. [CrossRef] [PubMed]